ISSN 1674-1056
http://cpb.iphy.ac.cn
http://iopscience.iop.org/cpb
中国物理 B
Chinese Physics
中国物理
Chinese Physics B

Hollow and filled fiber bragg gratings in nano-bore optical fibers

Yong-Xin Zhang(张永欣), Sheng Liang(梁生), Qian-Qing Yu(余倩卿), Zheng-Gang Lian(廉正刚), Zi-Nian Dong(董梓年), Xuan Wang(王旋), Yu-Qin Lin(林裕勤), Yu-Qi Zou(邹郁祁), Kun Xing(邢坤), Liu-Yan Liang(梁柳雁), Xiao-Ting Zhao(赵小艇), Li-Jing Tu(涂立静)

Citation: Chin. Phys. B . 2019, 28(7): 074210. **doi:** 10.1088/1674-1056/28/7/074210
Journal homepage: http://cpb.iphy.ac.cn; http://iopscience.iop.org/cpb

What follows is a list of articles you may be interested in

Cascaded tilted fiber Bragg grating for enhanced refractive index sensing

Biqiang Jiang(姜碧强), Zhixuan Bi(毕芷瑄), Shouheng Wang(王守恒), Teli Xi(席特立), Kaiming Zhou, Lin Zhang, Jianlin Zhao(赵建林)

Chin. Phys. B . 2018, 27(11): 114220. **doi:** 10.1088/1674-1056/27/11/114220

Gamma-radiation effects in pure-silica-core photonic crystal fiber

Wei Cai(蔡伟), Ningfang Song(宋凝芳), Jing Jin(金靖), Jingming Song(宋镜明), Wei Li(李伟), Wenyong Luo(罗文勇), Xiaobin Xu(徐小斌)

Chin. Phys. B . 2017, 26(11): 114211. **doi:** 10.1088/1674-1056/26/11/114211

Photon statistics of pulse-pumped four-wave mixing in fiber with weak signal injection

Nan-Nan Liu(刘楠楠), Yu-Hong Liu(刘宇宏), Jia-Min Li(李嘉敏), Xiao-Ying Li(李小英)

Chin. Phys. B . 2016, 25(7): 074203. **doi:** 10.1088/1674-1056/25/7/074203

Different supercontinuum generation processes in photonic crystal fibers pumped with a 1064-nm picosecond pulse

Chen Hong-Wei, Jin Ai-Jun, Chen Sheng-Ping, Hou Jing, Lu Qi-Sheng

Chin. Phys. B . 2013, 22(8): 084205. **doi:** 10.1088/1674-1056/22/8/084205

Optimization of highly nonlinear dispersion-flattened photonic crystal fiber for supercontinuum generation

Zhang Ya-Ni

Chin. Phys. B . 2013, 22(1): 014214. **doi:** 10.1088/1674-1056/22/1/014214

Hollow and filled fiber bragg gratings in nano-bore optical fibers*

Yong-Xin Zhang(张永欣)[1,†], Sheng Liang(梁生)[1,†,‡], Qian-Qing Yu(余倩卿)[2,3], Zheng-Gang Lian(廉正刚)[2], Zi-Nian Dong(董梓年)[1], Xuan Wang(王旋)[1], Yu-Qin Lin(林裕勤)[1], Yu-Qi Zou(邹郁祁)[1], Kun Xing(邢坤)[1], Liu-Yan Liang(梁柳雁)[1], Xiao-Ting Zhao(赵小艇)[4], and Li-Jing Tu(涂立静)[4]

[1] *Key Laboratory of Education Ministry on Luminescence and Optical Information Technology, National Physical Experiment Teaching Demonstration Center, Department of Physics, School of Science, Beijing Jiaotong University, Beijing* 100044, *China*
[2] *Yangtze Optical Electronic Company Ltd., Wuhan* 430205, *China*
[3] *Wuhan University of Technology, Wuhan* 430070, *China*
[4] *Anhui Agricultural University, Hefei* 230036, *China*

(Received 22 April 2019; revised manuscript received 21 May 2019; published online 3 July 2019)

To combine the technical functions and advantages of solid-core fiber Bragg gratings (FBGs) and hollow-core optical fibers (HCFs), the hollow and filled FBGs in nano-bore optical fibers (NBFs) with nano-bore in the GeO_2-doped core are proposed. The fundamental mode field, effective mode index, and confinement loss of NBF with 50 nm–7 μm-diameter hollow and filled nano-bore are numerically investigated by the finite element method. The reflected spectra of FBGs in NBFs are obtained by the transmission matrix method. The hollow FBGs in NBFs can be acheived with ∼ 5% power fraction in the bore and the ∼ 0.9 reflectivity when bore diameter is less than 3 μm. The filled FBGs can be realized with ∼ 1% power fraction and 0.98 reflectivity with different fillings including o-xylene, trichloroethylene, and chloroform for 800-nm bore diameter. The feasibility of the index sensing by our proposed NBF FBG is also analyzed and discussed. The experimental fabrication of hollow and filled FBGs are discussed and can be achieved by current techniques. The aim of this work is to establish a principle prototype for investigating the HCFs and solid-core FBGs-based fiber-optic platforms, which are useful for applications such as the simultaneous chemical and physical sensing at the same position.

Keywords: nano-bore optical fiber, fiber Bragg grating (FBG), hollow-core optical fiber (HCF), fiber optics

PACS: 42.81.–i, 42.81.Wg, 42.81.Dp **DOI:** 10.1088/1674-1056/28/7/074210

1. Introduction

Fiber Bragg grating (FBG) has delivered outstanding performance for applications in many fields of fiber-optic sensors, lasers, dispersion management, modulators, and filters, and has arrived at a high maturity level.[1–5] Recently the femtosecond-laser inscription technique[6,7] has effectively revolutionized the FBGs fabrication, and extended the applications to different types of optical fibers, as shown in Table 1.

The FBGs have been successfully inscribed in the index-guiding photonic crystal fiber (PCF) with the GeO_2-doped solid core[7] by the femtosecond-laser, and are also inscribed in the multi-core fibers for applications in sensors[8] and filters.[9] A novel CO_2 sensor at room temperature was proposed by using the FBG fabricated in the photo-sensitive optical fiber with the carbon nanotubes coated core.[10] A dual-peak FBG was inscribed in an all-solid photonic bandgap (PBG) fiber for sensing applications.[11] Furthermore, for the micro-structured optical fibers (MOFs) with solid core, FBGs have also been fabricated in the silica-polymer,[12] metallic-hole,[13] and small-hole[14,15] MOFs for applications in high-performance sensing.

Besides FBG written in the GeO_2-doped optical fibers, the high power ultraviolet and femtosecond laser have also been successfully applied to fabricating FBGs in the pure silica optical fibers. The FBGs can be inscribed in the suspended-core MOFs for applications in filters,[16] modulators,[17] and sensors.[18,19] Besides the suspended-core MOFs, FBG can also be fabricated in the pure silica solid core of MOFs with the random air-line cladding for structural health monitoring within nuclear reactors.[20] For the all-solid Bragg MOFs, the FBG can also be written in its GeO_2-doped and pure silica solid core by femtosecond laser for sensing.[21] The FBGs have been inscribed in the solid core with GeO_2-doped rods array in a nanostructure core fiber,[22] in the solid hydrogen loaded silica core of dual-core MOF,[23] and in the hollow eccentric fiber.[24] Besides the photosensitivity, the femtosecond laser ablation drilled periodic nano-holes can also be utilized in the exposed core MOFs and microfibers.[25,26]

Currently, for both the conventional step-index optical fibers and various different MOFs, FBGs are all written in the solid cores.[1–26] It is obvious that the FBGs cannot be fabricated in the hollow core (HC) of optical fiber. Therefore, there is little work on the attempt at combining the technical functions and advantages of both solid-core FBGs and hollow-core optical fibers (HCFs).

*Project supported by the Beijing Natural Science Foundation, China (Grant No. 4192047), the Fundamental Research Funds for the Central Universities, China (Grant Nos. 2018JBM070 and 2018JBM065), and the National Natural Science Foundation of China (Grant No. 61675019).

†These authors contributed equally to this work.
‡Corresponding author. E-mail: shliang@bjtu.edu.cn

© 2019 Chinese Physical Society and IOP Publishing Ltd

Table 1. State-of-the-art of FBGs fabricated in different optical fibers.

Ref.	Optical fibers	Applications	Cores
[1]	step-index fiber	various	GeO_2-doped, solid
[2]	step-index fiber	sensor	GeO_2-doped, solid
[3]	HB step-index fiber	sensor	GeO_2-doped, solid
[4]	step-index fiber	sensor	GeO_2-doped, solid
[5]	step-index fiber	sensor	GeO_2-doped, solid
[6]	step-index fiber	various	GeO_2-doped, solid
[7]	index-guiding PCF	various	GeO_2-doped, solid
[8]	multicore fiber	sensor	GeO_2-doped, solid
[9]	multicore fiber	filter	GeO_2-doped, solid
[10]	coated core fiber	sensor	GeO_2-doped, solid
[11]	all-solid PBG MOF	sensor	GeO_2-doped, solid
[12]	air-hole cladding MOF	sensor	GeO_2-doped, solid
[13]	metallic-hole MOF	sensor	GeO_2-doped, solid
[14]	small-hole MOF	sensor	GeO_2-doped, solid
[15]	multi-core PCF	sensor	pure silica, solid
[16]	suspended-core MOF	filter	pure silica, solid
[17]	suspended-core MOF	modulator	pure silica, solid
[18]	suspended-core MOF	sensor	pure silica, solid
[19]	suspended-core MOF	sensor	pure silica, solid
[20]	random clad MOF	sensor	pure silica, solid
[21]	all-solid Bragg MOF	sensor	GeO_2-doped & pure silica, solid
[22]	nanostructure core fiber	sensor	GeO_2-doped rods array, solid
[23]	dual-core MOF	sensor	hydrogen loaded silica, solid
[24]	hollow eccentric fiber	sensor	hydrogen loaded silica, solid
[25]	exposed core MOF	sensor	silica, solid with drilled holes
[26]	micro-fiber	various	silica, solid with drilledc holes
This work	nano-bore fiber	various	GeO_2-doped, with nano-bore

However, the lately proposed special optical fibers, namely, the nano-bore optical fibers (NBFs)[27–30] may produce the possibility to make a breakthrough. The NBF consists of a GeO_2-doped core, a silica cladding, and a central hollow nano-bore in the core.[27–30] Several NBFs have been reported as shown in Table 2. The NBFs with step-index and GeO_2-doped cores have been proposed with air,[27] liquid,[27,28] dielectric particles,[29] and gold nano-wire[30] in the nano-bore for applications in sensing,[27] spectroscopy,[28] nanoparticle tracking,[29] plasmonics, and optics.[30] Even a nano-bore with a 20-nm diameter was successfully fabricated in the solid core of a soft glass MOFs for sensing and nonlinear optics.[31] What is more, the silica-chalcogenide NBFs with thermo-optic liquid filled single[32] and dual[33] nano-bores have also been numerically and experimentally demonstrated for applications in parametric sources, light–matter interaction, and spatial soliton propagation.

Table 2. Current work on NBFs.

Ref.	Optical fibers	Cores	D_{bore}/nm	Filling in bores	Applications
[27]	step-index fiber	GeO_2-doped	$180 \sim 940$	air and liquids	sensors
[28]	step-index fiber	GeO_2-doped	600	liquid	spectroscopy
[29]	step-index fiber	GeO_2-doped	247 ± 6	dielectric particles	nanoparticle tracking
[30]	step-index fiber	GeO_2-doped	1100	gold nano-wire	Plasmonics & Optics
[31]	soft glass MOF	soft glass	$20 \sim 150$	air	sensing & nonlinearity
[32]	silica-chalcogenide	chalcogenide	$200 \sim 1600$	thermo-optic liquid	parametric sources
[33]	silica-chalcogenide	chalcogenide	$500 \sim 1000$	thermo-optic liquid	light-matter interaction

Current work on NBFs focuses on taking full advantages of selective filling and maintaining total internal reflection in the core with the nano-bore. However, the NBFs make possible the hollow and filled FBGs due to the presence of both solid GeO_2-doped core and the hollow nano-bore. In this paper, hollow and filled FBGs in the NBFs are proposed and investigated in detail to attempt to integrate the FBGs and HCFs together.

2. Nano-bore optical fiber

The NBF studied here is based on a silica step-index optical fiber, and consists of a GeO_2-doped silica core, and a silica cladding, and there is a central hollow nano-channel extending through the entire length of the NBF as shown in Fig. 1.

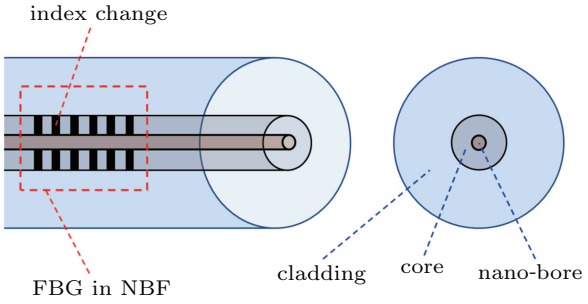


Fig. 1. Sketch of NBF consisting of a GeO_2-doped core, silica cladding, central hollow nano-channel,[27–30] and FBG in NBF.

The diameters of the cladding and the core of NBF are $D_{\text{cladding}} = 125$ μm and $D_{\text{core}} = 8$ μm, respectively. The diameter of the nano-bore D_{bore} changes from 50 nm to 7 μm in our numerical investigations. The refractive index of the silica cladding is $n_{\text{cladding}} = 1.45$ for 1550-nm wavelength. The GeO_2-doped concentration in the core is 5.3 mol%, then, the refractive index difference between core and cladding is 8×10^{-3}, therefore, the refractive index of the core is $n_{\text{core}} = 1.458$. The refractive index of the hollow nano-bore is $n_{\text{bore}} = 1$. It is worth noticing that the high Ge-content can offer intrinsic photosensitivity for FBG inscription without hydrogenation.

Here, we analyze several application-relevant properties of the NBFs by the full-vector finite element method (FEM),[34] including the fundamental mode field, the confinement loss, and effective mode index of the fundamental mode with different nano-bore diameters. The obtained results will pave the way for fabrication of FBGs in the NBFs.

The fundamental mode fields of NBFs with different nano-bore diameters when the wavelength is 1550 nm and $n_{\text{bore}} = 1$ are shown in Fig. 2. The results are all for 1550-nm wavelength and a hollow nano-bore ($n_{\text{bore}} = 1$). The values of effective index n_{eff} of the fundamental mode with different values of bore diameter D_{bore} are illustrated in Fig. 3. When D_{bore} increases, n_{eff} decreases due to the decrease of the proportion of silica in the core.

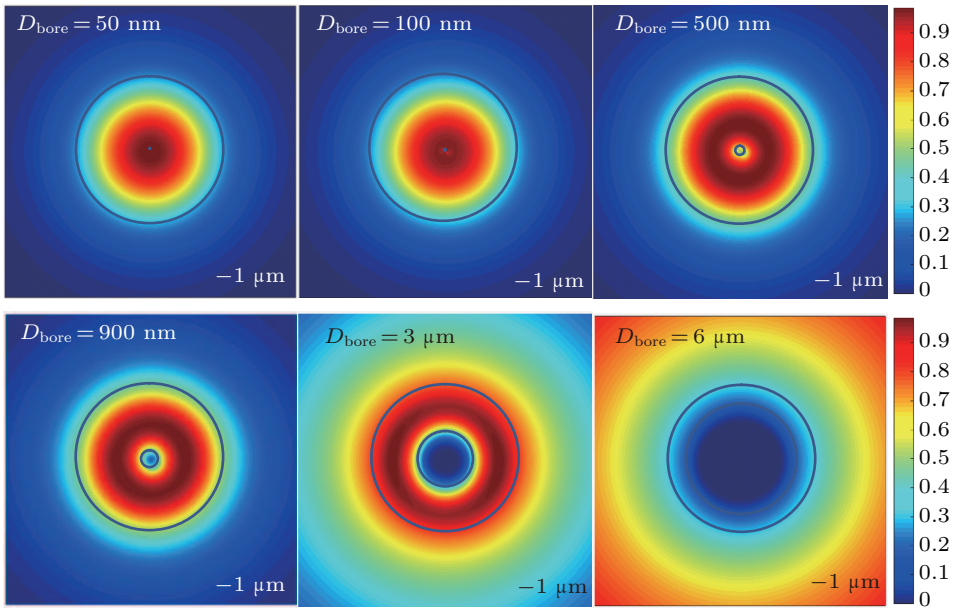


Fig. 2. Images for normalized electric field intensity of fundamental mode in NBF with different bore diameters.

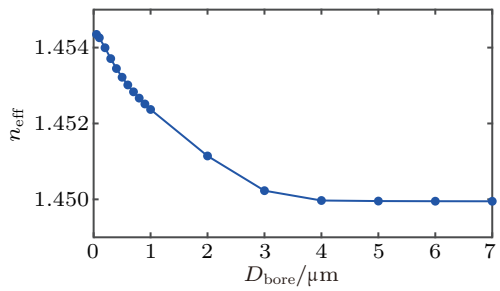


Fig. 3. Variation of effective index of fundamental mode (n_{eff}) with bore diameter (D_{bore}).

Then, the confinement loss of fundamental mode (α) as a function of D_{bore} is illustrated in Fig. 4. For the NBF with hollow bore, when $D_{\text{bore}} < 1$ μm, thers is no obvious confinement loss, however, α increases remarkably from 5.85 dB/m to 10.62 dB/m when $D_{\text{bore}} \geq 3$ μm.

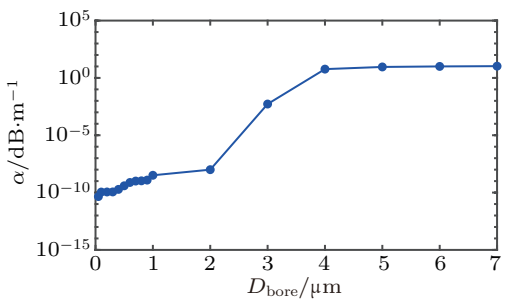


Fig. 4. Plot of confinement loss (α) of fundamental mode *versus* nano-bore diameter (D_{bore}).

Then the cross section of the normalized intensity of the mode field is shown in Fig. 5. In order to quantitatively describe the power in the bore, an important parameter, power fraction (η), is used, which represents the ratio of the power inside the nano-bore to the total guided power of the fundamental mode, and η can be obtained by integrating the z-component of Poynting vector (S_z) in the bore (A_{bore}) and the core (A_{core}) domains, as follows:

$$\eta = \int A_{\text{bore}} S_z \, \mathrm{d}A \Big/ \int A_{\text{core}} S_z \, \mathrm{d}A. \tag{1}$$

Then, the power fraction (η) of NBFs as a function of bore diameter (D_{bore}) is illustrated in Fig. 6. It goes without saying that η increases with D_{bore} increasing.

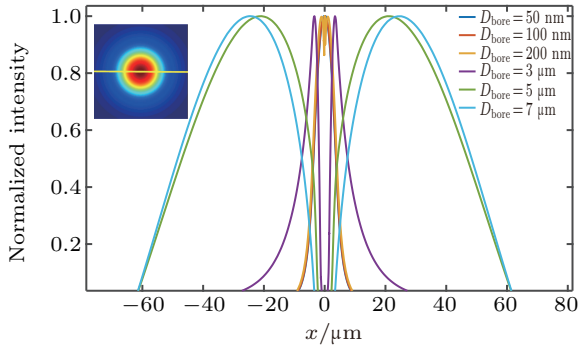


Fig. 5. Plots of cross section of normalized mode field intensity *versus* position in x direction for different values of bore diameter (D_{bore}).

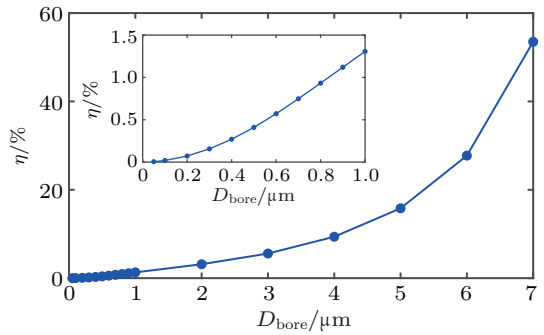


Fig. 6. Plot of power fraction (η) of NBFs (8-μm core diameter) with hollow bore *versus* bore diameter (D_{bore}).

The power fraction η lies in a range between 0.0047% and 1.2101% when D_{bore} increases from 50 nm to 900 nm, suggesting that the influence of the lossis negligible as long as fiber length below about 10 cm is considered. When D_{bore} is in a range of 1 μm–4 μm, the power fraction η observably increases from 1.3071% to 9.3734%. Furthermore, there is a high η value of 53.5030% in the case of 7-μm D_{bore}. It is necessary to note that they are very special cases where $D_{\text{bore}} = 5$ μm and 7 μm in Fig. 5. The most of the intensity is outside the core, which leads to a very low reflectivity of FBG as shown in Fig. 7 (see below). There is very little light in the bore, and also in the core, therefore, there is a relatively high η when D_{bore} is larger than 5 μm.

Larger bore can lead to the high power fraction, which is useful for enhancing the light–matter interation, the sensitivity of the absorption spectrum and chemical sensing, and the power fraction can be enhanced to $\sim 30\%$ by arranging the geometric parameter and selective filling.[35] However, the larger D_{bore} also brings in the high confinement loss, and the characteristic of FBG in NBF may be degenerated, which will be studied in the next section.

3. Hollow FBG in NBF with hollow nano-bore

The FBG can be inscribed in the GeO_2-doped and solid part of NBF core as shown in Fig. 1. Generally, a uniform FBG can be described by a modulation of the effective refractive index ($n(z)$) of the fundamental guided mode along the fiber axis z. The $n(z)$ is given as follows:

$$n(z) = n_{\text{eff}} \left\{ 1 + \frac{\Delta n_{\text{eff}}}{n_{\text{eff}}} \left[1 + \cos\left(\frac{2\pi}{\Lambda_0} z \right) \right] \right\},$$
$$z \in \left[-\frac{L}{2}, \frac{L}{2} \right], \tag{2}$$

where n_{eff} is the unperturbed effective index of the fundamental mode, Δn_{eff} is the "DC" index change spatially averaged over a grating period, L is the grating length, and $L = 2$ cm in our simulation, and $\Lambda = 536$ nm is the grating period. In order to suppress the sidelobes in the reflected spectrum, we use the "raised-cosine" apodization here.

With the purpose of carrying out the numerical analysis of the FBG in NBF, the coupled mode theory based transfer matrix method (TMM)[1] is utilized by taking into account the existence of the nano-bore. The FBG is based on the photosensitivity, which is described as the light-induced permanent effective refractive index change. In most of cases, the photosensitivity of single-mode fiber is initiated by the breaking of Ge–Si bonds with UV radiation,[36] which is strongly supported by hydrogen loading.[37] A general value of Δn_{eff} for simulation is $\Delta n_{\text{eff0}} = 2.19 \times 10^{-4}$.[38] However, for the FBG in NBF, the index Δn_{eff} is reduced due to the nano-bore in the core, and is approximately estimated in our simulatiom from

$$\Delta n_{\text{eff}} = \Delta n_{\text{eff0}} \times (1 - D_{\text{bore}}^2 / D_{\text{core}}^2). \tag{3}$$

The reduced index change described by Eq. (3), is based on the assumption that the index change is proportional to the area ratio between solid and the whole core, which is valid for an FBG length of several centimeters. What is more, it is needed to note that when calculating the reflected spectrum of FBG, the confinement loss due to the 5-cm length of the NBF is added to describe the NBF pigtail in the practical applications.

Then, the reflected spectra of FBG in NBF with different bore diameters are shown in Fig. 7. Furthermore, to observe the spectra more quantitatively, the maximum reflectivity (R_{max}) and the Bragg wavelength (λ_{B}) with different values

of D_{bore} are shown in Figs. 8 and 9, respectively. It is found that for D_{bore} in a range from 50 nm to 3 μm, $R_{\max}$ keeps more than 85%, however, when $D_{\text{bore}} \geq 4$ μm, $R_{\max}$ descreases quickly; even for $D_{\text{bore}} = 7$ μm, $R_{\max}$ is 0, which means that there is no available FBG in NBF. The reason is that when D_{bore} increases, the confinement loss is enhanced, meanwhile, the solid part of the core is also reduced, which remarkably weakens the index changing for forming the FBG and also the diffraction by FBG.

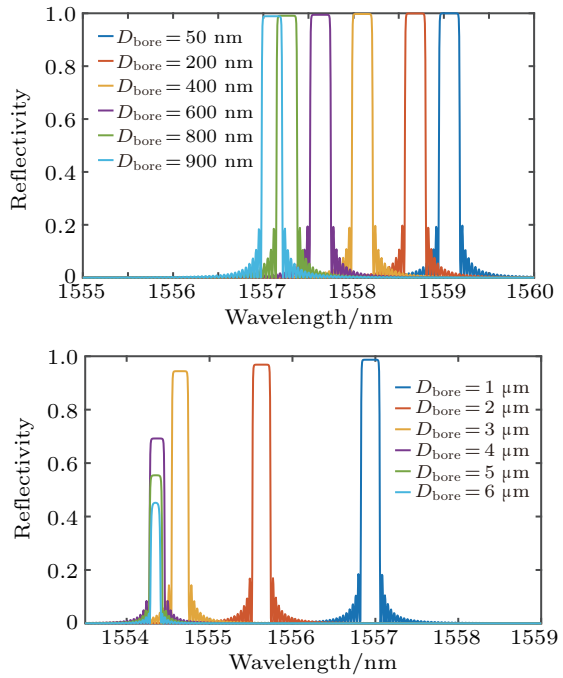


Fig. 7. Reflected spectra of hollow FBG in NBF for different bore diameters.

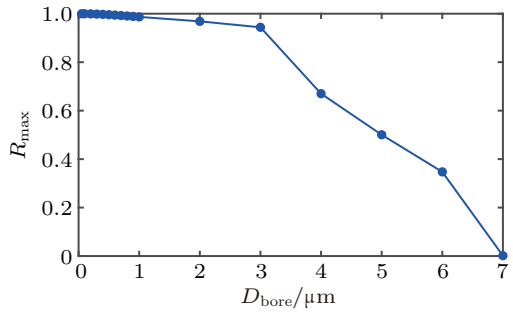


Fig. 8. Variation of maximum reflectivity ($R_{\max}$) *versus* bore diameter (D_{bore}) of FBG.

From Fig. 9, it is found that λ_B shows similar dependence on D_{bore} to n_{eff} as shown in Fig. 3, due to the quantitative relationship between λ_B and effective index of FBG[1]

$$\lambda_B = 2n_{\text{effFBG}} \cdot \Lambda, \tag{4}$$

where n_{effFBG} denotes the effective index of FBG, different from that of the fundamental mode (n_{eff}). However, not only n_{eff} but also Δn_{eff} is changed by different D_{bore} values, so, λ_B changes more obviously than n_{eff} due to D_{bore} changing.

It is found that the hollow FBG in NBFs can be realized with ~ 80% reflectivity, and the hollow bore for selective filling will be studied in the next section in detail.

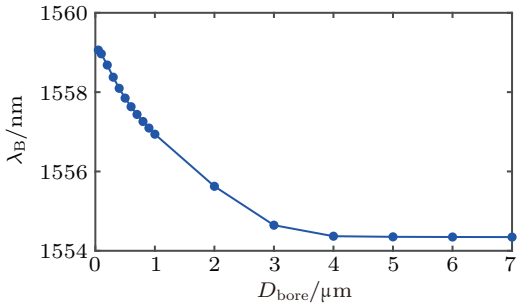


Fig. 9. Variation of Bragg wavelength (λ_B) of FBG with bore diameter (D_{bore}).

4. Filled FBG in NBF with filled nano-bore

The filled FBG in NBF can be realized by selective filling in the bore. We choose three different fillings including o-xylene, trichloroethylene, and chloroform[39] with different values of effective index (n_{filling}), which are less and greater than the index of core (1.458). It is noted that the fluctuation of n_{filling} with the change of wavelength is ignored.

The effective mode index (n_{eff}) and power fraction (η) of the filled NBF, the maximal reflectivity ($R_{\max}$), and Bragg wavelength (λ_B) of filled FBG are shown in Table 3. The material induced attenuation of filling is ignored.

The effective mode index n_{eff} increases when D_{bore} changes from 300 nm to 800 nm for o-xylene and trichloroethylene with the index n_{filling} greater than core index. By contraries, n_{eff} decreases with larger D_{bore} for chloroform with n_{filling} less than core index. The power fraction η for $D_{\text{bore}} = 800$ nm is 10 times larger that for $D_{\text{bore}} = 300$ nm. The reflected spectra of filled FBGs and fundamental mode field of NBFs with different bore diameters and fillings are illustrated in Fig. 10. It is obvious that the light confinement is enhanced by both the increased n_{eff}, and the larger D_{bore} for the xylene and trichloroethylene due to their greater n_{filling}. In the cases of these three fillings with 300-nm and 800-nm bore diameters, $R_{\max}$ maintains greater than 0.98.

In the case of the o-xylene, trichloroethylene, and chloroform filled NBF with 800-nm D_{bore}, the power fraction η can reach ~ 1%. This value is effective for absorption spectrum to detect high-concentration analytes at experimentally feasible length, which is hard for current cuvette-based experiments. For a power fraction factor of 0.1%, a 1-cm-long NBF allows measuring a 1000-times higher analyte concentration than a 1-cm-long cuvette.[28] What is more, it is interesting to find that the bore with 1% η can be utilized in absorption spectroscopy and chemical sensing, and the GeO_2-doped and solid part of core leads to the FBGs with high reflectivity, which means that a filled FBG can be realized.

Table 3. Filled FBGs in NBFs with different fillings and D_{bore} values.

Filling	$n_{filling}$	D_{bore}/nm	n_{eff}	η/%	R_{max}	λ_B/nm
o-xylene	1.4846	300	1.4544	0.1733	0.9982	1559.2
		800	1.4549	1.3461	0.9865	1559.7
Trichloroethylene	1.4601	300	1.4543	0.1716	0.9982	1559.1
		800	1.4544	1.2262	0.9877	1559.1
Chloroform	1.4321	300	1.4543	0.1698	0.9982	1559.0
		800	1.4540	1.1555	0.9884	1558.7

In order to analyze the feasibility of the index sensing by the NBF FBG, the equivalent wavelength sensitivity S_λ of the Bragg wavelength to the filled index can be calculated from

$$S_\lambda = \Delta\lambda_B/\Delta n_{filling}, \tag{5}$$

where $\Delta\lambda_B$ and $\Delta n_{filling}$ are the change of Bragg wavelength and the filled index, respectively. Then, the equivalent wavelength sensitivities with different bore diameters are shown in Table 4.

Table 4. Equivalent sensitivities with different bore diameters. RIU: refractive index unit.

D_{bore}/nm)	S_λ/(nm/RIU*)
300	(1559.2–1559.0)/(1.4846–1.4321)= 3.8095
800	(1559.7–1559.0)/(1.4846–1.4321)= 13.3333

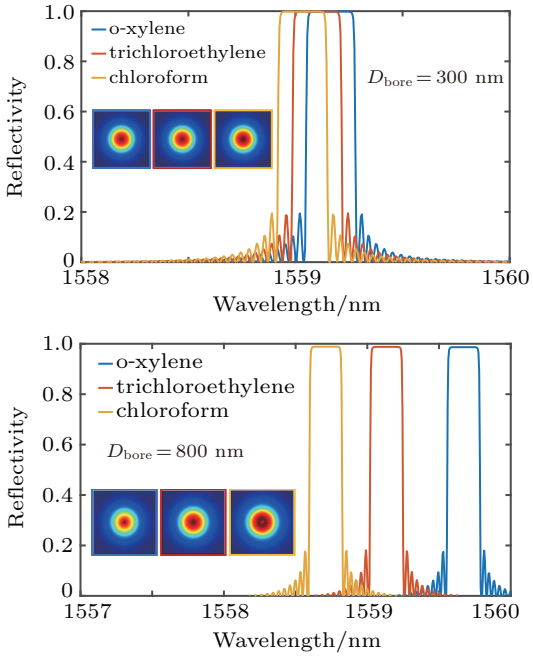


Fig. 10. Reflected spectra of filled FBG and fundamental mode field of NBF with different bore diameters and fillings.

5. Discussion on experimental verification and applications

The NBF can be fabricated by thermally drawning the centimeter-thick fused silica and preformed with a GeO_2-doped core and a hollow central channel at high temperatures into a fiber.[27–30] Then, the uniform FBGs in NBF can be fabricated by the phase-mask scanning technique,[38,40] where the 248-nm UV radiation from a frequency-doubled argon laser is focused by a cylindrical lens through a uniform phase mask onto the core of NBF. However, the existence of the hollow bore in the core will strongly defocus the UV beams, especially for the large bores. We believe that it may be an effective solution to fill the bore with the suitable material with high index nearly the same as the index of the GeO_2-doped core and low loss for UV beams during the exposure progress. Furthermore, the power of the UV laser and the scanning speed need optimizing for different bore diameters for the cases with or without the hydrogen-loading. In order to improve the long-term reliability of FBG in NBF, the annealing may also need implementing for practical applications. These engineering issues will be studied in our future work.

For applications in sensing, the chemical patameters such as solution concentration, relative humidity, and hydrogen concentration can be measured by employing our proposed NBF FBG as a refractive index sensor by filling the analyte in the hollow and selective coating (hydrogel humidity for and palladium for hydrogen) bores. The physical parameters including strain and temperature can also be detected by our proposed FBG in NBF.

6. Conclusions

In this paper, we report the detailed theoretical investigations of hollow and filled FBGs in the NBFs, which is an integration of HCFs and FBGs. The GeO_2-doped solid part of the core in NBF is employed to fabricate FBG, and the nano-bore of the NBF core can be selectively filled, to form a hollow or filled FBG. By the full-vector FEM, the transmission characteristics including the fundamental mode field, effective mode index, and confinement loss of NBF with different-diameter hollow and filled nano-bore are numerically investigated. Then, the reflected spectra of FBGs in the NBFs are obtained by the TMM, based on the numerical results of NBF transmission characteristics. The range of bore diameter for available power fraction in the bore and the range of FBG reflectivity are obtained. For the hollow FBGs, the $\sim 5\%$ power fraction in the bore and the ~ 0.9 reflectivity can be realized with < 3-μm bore diameter. For the filled FBGs, the $\sim 1\%$ power fraction and 0.98 reflectivity with different fillings including o-xylene, trichloroethylene, and chloroform can be achieved by using an 800-nm bore diameter. The feasibility of the index sensing by our proposed NBF FBG is analyzed and discussed. We believe that this work is a useful reference for the integrated fiber-optic platforms with HCFs and FBGs.

References

[1] Erdogan T 1997 *J. Lightwave Technol.* **15** 1277
[2] Tosi D 2018 *Sensors* **18** 2147
[3] Caucheteur C, Guo T and Albert J 2017 *J. Lightwave Technol.* **35** 3311

[4] Wen S Z, Xiong W C, Huang L P, Wang Z R, Zhang X B and He Z H 2018 *Chin. Phys. B* **27** 090701
[5] Jiang B Q, Bi Z X, Wang S H, Xi T L, Zhou K M, Zhang L and Zhao J L 2018 *Chin. Phys. B* **27** 114220
[6] Mihailov S J, Smelser C W, Lu P, Walker R B, Grobnic D, Ding H M, Henderson G and Unruh J 2003 *Opt. Lett.* **28** 995
[7] Baghdasaryan T, Geernart T, Morana A, Marin E, Girard S, Makara M, Mergo P, Thienpont H and Berghmans F 2018 *Opt. Express* **26** 14741
[8] Dochow S, Latka I, Becker M, Spittel R, Kobelke J, Schuster K, Graf A, Brückner S, Unger S, Rothhardt M, Dietzek B, Krafft C and Popp J 2012 *Opt. Express* **20** 20156
[9] Birks T A, Mangan B J, Diez A, Cruz J L and Murphy D F 2012 *Opt. Express* **20** 13996
[10] Shivananju B N, Yamdagni S, Fazuldeen R, Kumar A K S, Hegde G M, Varma M M and Asokan S 2013 *Rev. Sci. Instrum.* **84** 065002
[11] Zhang J H, Liu N L, Wang Y, Ji L L and Lu P X 2012 *Chin. Phys. Lett.* **29** 074205
[12] Berghmans F, Geernaert T, Baghdasaryan T and Thienpont H 2014 *Laser & Photon. Rev.* **8** 27
[13] Wang J, Liu Z Y, Gao S R, Zhang A P, Shen Y H and Tam H Y 2016 *J. Lightwave Technol.* **34** 4884
[14] Zhang A P, Yan G F, Gao S R, He S L, Kim B, Im J and Chung Y 2011 *Appl. Phys. Lett.* **98** 221109
[15] Xiang H L and Jiang Y J 2018 *OPTIK* **171** 9
[16] Silva R E, Becker M, Rothhardt M, Bartelt H and Pohl A A P 2017 *IEEE Photon. J.* **9** 7801209
[17] Da Silva R E, Becker M, Rothhardt M, Bartelt H and Pohl A A P 2018 *J. Lightwave Technol.* **36** 4146
[18] Wang C, He J, Zhang J C, Liao C R, Wang Y, Jin W, Wang Y P and Wang J H 2017 *Opt. Express* **25** 28442
[19] Wang C, Zhang J C, Zhang C Z, He J, Lin Y C, Jin W, Liao C R, Wang Y and Wang Y P 2018 *J. Lightwave Technol.* **36** 2920
[20] Mihailov S J, Hnatovsky C, Grobnic D, Chen K and Li M J 2018 *IEEE Photon. Technol. Lett.* **30** 209
[21] Li Y H, Chen W, Wang H Y, Liu N L and Lu P X 2011 *J. Lightwave Technol.* **29** 3367
[22] Yu X, Yan M, Ren G B, Tong W J, Cheng X P, Zhou J Q, Shum P P and Ngo N Q 2009 *J. Lightwave Technol.* **27** 1548
[23] Zhang X P and Peng W 2015 *IEEE Photon. Technol. Lett.* **27** 391
[24] Mao G P, Yuan T T, Guan C Y, Yang J, Chen L, Zhu Z, Shi J H and Yuan L B 2017 *Opt. Express* **25** 144
[25] Warren-Smith S C and Monro T M 2014 *Opt. Express* **22** 1480
[26] Zhao P, Li Y H, Zhang J H, Shi L and Zhang X L 2012 *Opt. Express* **20** 28625
[27] Schaarschmidt K, Weidlich S, Reul D and Schmidt M A 2018 *Opt. Lett.* **43** 4192
[28] Jiang S, Schaarschmidt K, Weidlich S and Schmidt M A 2018 *J. Lightwave Technol.* **36** 3970
[29] Faez S, Lahini Y, Weidlich S, Garmann R F, Wondraczek K, Zeisberger M, Schmidt M A, Orrit M and Manoharan V N 2015 *ACS Nano* **9** 12349
[30] Tuniz A, Jain C, Weidlich S and Schmidt M A 2016 *Opt. Lett.* **41** 448
[31] Ruan Y L, Ebendorff-Heidepriem H, Afshar S and Monro T M 2010 *Opt. Express* **18** 26018
[32] Singh S P, Mishra V, Datta P K and Varshney S K 2015 *J. Lightwave Technol.* **33** 55
[33] Mishra V, Singh S P, Haldar R and Varshney S K 2016 *IEEE J. Sel. Top. Quantum Electron.* **22** 208
[34] Cucinotta A, Selleri S, Vincetti L and Zoboli M 2002 *J. Lightwave Technol.* **20** 1433
[35] Ruan Y, Afshar S and Monro T M 2011 *IEEE Photon. J.* **3** 130
[36] Limberger H G, Fonjallaz P Y, Salathe R P and Cochet F 1996 *Appl. Phys. Lett.* **68** 3069
[37] Riant I and Poumellec B 1998 *Electron. Lett.* **34** 1603
[38] Liang S, Tjin S C, Ngo N Q, Zhang C X and Li L J 2009 *Opt. Commun.* **282** 1363
[39] Saunders J E, Sanders C, Chen H and Loock H P 2016 *Appl. Opt.* **55** 947
[40] Malo B, Theriault S, Johnson D C, Bilodeau F, Albert J and Hill K O 1995 *Electron. Lett.* **31** 223